Evaluation of a multi-satellite soil moisture product and the Community Land Model 4.5 simulation in China

Binghao Jia[1], Jianguo Liu[1,2] and Zhenghui Xie[1]

[1] {*State Key Laboratory of Numerical Modeling for Atmospheric Sciences and Geophysical Fluid Dynamics (LASG), Institute of Atmospheric Physics, Chinese Academy of Sciences, Beijing, China*}
[2] {*High Performance Computing Center, Department of Mathematics and Applied Mathematics, Huaihua University, Huaihua, Hunan, China*}

Correspondence to: Jianguo Liu (jgliu@mail.iap.ac.cn)

Submitted to *Hydrology and Earth System Sciences*

5 May 2015 − Revised: 21 August 2015

Abstract

Twenty years of in situ soil moisture data from 306 stations located in China were used to perform an evaluation of two surface soil moisture datasets: (1) a microwave-based multi-satellite product (ESA CCI SM) and (2) soil moisture estimations from the Community Land Model 4.5 (CLM4.5), forced by observation-based atmospheric forcing data. Both soil moisture products generally showed a good agreement with in situ observations, with unbiased root mean square differences (ubRMSD) of 0.05 m^3 m^{-3}. The average Spearman rank correlation coefficient (R_{sp}) between the ESA CCI SM product and all in situ observations was 0.37. In contrast, the CLM4.5 model produced better temporal variation of surface soil moisture (R_{sp} = 0.42) than the ESA CCI SM product, but showed larger ubRMSD in southwestern China, which may have been related to inaccurate precipitation data. The ESA CCI SM product is more likely to be superior to the CLM4.5 model in semi-arid regions, mainly because of the accurate data retrievals and high observation density, but inferior over areas covered by dense vegetation. Furthermore, the ESA CCI SM product showed a stable to

slightly better performance in China over time, except for a decline in performance during 2007–2010, when different data for the satellite product were blended. Results from this study can provide comprehensive insight into the performances of the two soil moisture datasets in China, which will facilitate improvements in merging algorithms or model simulations and for applications in soil moisture data assimilation.

Key words: soil moisture, remote sensing, CLM4.5, essential climate variable

1. Introduction

Soil moisture is a key variable in hydrological, climatological, biological and ecological processes. It is central to land–atmosphere interactions because of its control on the partitioning of water and energy fluxes at the Earth's surface (Dai et al., 2004). Soil moisture also affects the seasonal and inter-annual dynamics of vegetation, which is an essential component of the coupled hydrological and carbon cycles (Ciais et al., 2005). Many studies have been conducted to obtain estimates of soil moisture using remote sensing techniques (Njoku et al., 2003; Owe et al., 2008; Kerr et al., 2012), land surface modeling (Dirmeyer et al., 2006; Wang et al., 2011; Liu and Xie, 2013) or a combination of both through a land data assimilation system (e.g., Dharssi et al., 2011, de Rosnay et al., 2013).

Spaceborne microwave instruments can provide quantitative information about surface soil water content (Schmugge, 1983), particularly in the low-frequency microwave region from 1 to 10 GHz (Albergel et al., 2012). Several microwave-based soil moisture datasets have been generated using satellite data retrievals from active microwave sensors, e.g. the European Remote Sensing Satellites 1 and 2 Active Microwave Instrument Wind Scatterometer (AMI-WS; Scipal et al., 2002) and Advanced SCATterometer (ASCAT) onboard the Meteorological Operational satellite program (MetOp; Bartalis et al., 2007), and from passive microwave sensors, including the Scanning Multichannel Microwave Radiometer (SMMR; Owe et al., 2008), the Special Sensor Microwave Imager (SSM/I) of the

Defense Meteorological Satellite Program (DMSP; Owe et al., 2008), the Tropical Rainfall Measuring Mission microwave imager (TMI; Jackson and Hsu, 2001; Gao et al., 2006; Owe et al., 2008), and more recently the Advanced Microwave Scanning Radiometer–Earth observing system (AMSR-E) onboard the Aqua satellite (Njoku et al., 2003; Owe et al., 2008). The AMSR-E radiometer was switched off in October 2011 because of rotation problems with its antenna; however, the AMSR2, launched in May 2012 onboard the Global Change Observation Mission 1–Water (GCOM–W1), was intended to extend its valuable heritage (Parinussa et al., 2015). Even though none of these sensors were specifically designed for measuring soil moisture, good correspondences have been found between the individual datasets and ground-based observations taken over a large variety of environmental conditions (Albergel et al., 2009, 2012; Draper et al., 2009; Gruhier et al., 2010; Brocca et al., 2011).

However, none of the individual microwave products cover the decadal timescales required to be considered for use in climate applications. Recently, a multi-satellite soil moisture dataset (ESA CCI SM) spanning over thirty years was constructed by merging two active and six passive microwave products (Liu et al., 2011, 2012). The combined product, which was initially developed under the European Space Agency (ESA) Water Cycle Multi-Mission Observation Strategy (WACMOS) project, is now being extended and improved within the Climate Change Initiative (CCI) (http://www.esa-soilmoisture-cci.org/; Wagner et al., 2012). A few studies have evaluated the ESA CCI SM product using in situ observations. Liu et al. (2011, 2012) indicated that the merged dataset had a similar accuracy to that of the best input product but with an increased temporal sampling density. Albergel et al. (2013a) found that the ESA CCI SM dataset agreed well with in situ measurements between 2007 and 2010 for 196 sites from five networks across the world, but that its performance over most networks remained poorer than that of the most recent reanalysis

products. Dorigo et al. (2015) provided a more in-depth evaluation; they used 596 stations from 28 historical and active monitoring networks worldwide. Whilst the performance of the ESA CCI SM dataset appeared to be relatively stable over time, large discrepancies were observed among different networks. In addition, the ESA CCI SM can also capture long-term systematic changes in trends of ground-based observations (Dorigo et al., 2012; Albergel et al., 2013b), which suggests that it has a large potential for climate trend assessments (Loew et al., 2013).

China has the third largest land area and diverse climates and biomes. Previous studies have used only 34 sites for the period 1981–2000 across China and only 20 sites for the period 2008–2010 from the Maqu network in northwest China to investigate the performance of the ESA CCI SM product (Albergel et al., 2013a; Dorigo et al., 2015). Such sparse observations clearly affect the evaluation results, leading to large uncertainties. Recently, Chinese soil moisture observations for 306 sites from 1993 were updated by the China Meteorological Administration (CMA) National Meteorological Information Center (NMIC). These data have been extensively used to investigate the variations of soil moisture and evaluate the land surface modeling (Li et al, 2005; Wang and Zeng, 2011; Liu and Xie, 2013).

Land surface modeling is another strategy to produce large-scale surface and root zone soil moisture estimations. When forced by high quality atmospheric forcing data, this strategy has proved to be an effective tool to complement the commonly use of in situ measurements and for the evaluation of satellite retrievals at both regional and global scales (Albergel et al., 2010, 2012). The ESA CCI SM product has also demonstrated a potential for evaluating climate model performances (Loew et al, 2013; Szczypta et al., 2014). As one of the state-of-art land surface models, the Community Land Model version 4.5 (CLM4.5) from the National Center for Atmospheric Research (NCAR) was released in 2013 (Oleson et al.,

2013). To our knowledge, few studies have focused on the performance of CLM4.5 soil moisture simulations in China. Lai et al. (2015) validated the temporal variation of soil moisture simulated from the CLM4.0, a previous version of CLM4.5, but used only 30 sites to cover China for the period 1981–1999; they also compared the spatial variation of soil moisture in China using the ESA CCI SM product. However, the performance of the ESA CCI SM product was not discussed in their work.

In this study, we conducted an in-depth evaluation of the ESA CCI SM product and CLM4.5 simulation in China using ground-based observations from 306 sites. We investigated their performances over various sub-regions under different climate conditions. This in-depth evaluation provided a better understanding of the quality of both soil moisture products and their potential problems than was hereafter available, and can be used to improve their accuracy. The soil moisture datasets used in this study and the methodology for their evaluation are described in Section 2. The results and discussion are then presented in Section 3 and Section 4, respectively. Finally, our conclusions are given in Section 5.

2. Material and methods

2.1 Community Land Model (CLM4.5)

The NCAR/CLM is a community-developed model for simulating land surface processes, such as water, energy, and carbon fluxes. The CLM4.5 version is the latest of the CLM family of models (Oleson et al., 2013). It contains several notable improvements over previous releases, including the decrease of biases associated with the modeled terrestrial carbon cycle and modifications of canopy and hydrology processes (Oleson et al. 2013). In CLM4.5, spatial land surface heterogeneity is represented as a nested subgrid hierarchy in which grid cells are composed of multiple land units, snow/soil columns, and plant functional types (PFTs). The model has one vegetation layer, fifteen layers for soil and up to five layers for snow, depending on snow depth. The soil depths for the uppermost five layers are 1.75,

4.51, 9.06, 16.55 and 28.91 cm. For soil points, temperature calculations are performed over all layers, but hydrology calculations are performed over the top 10 layers only; the bottom five layers are classified as bedrock. A detailed description of the physical processes included within CLM4.5 can be found in Oleson et al. (2013). It should be noted that although CLM4.5 includes the option to be operated with a dynamic vegetation or prognostic carbon-nitrogen model, in our study, CLM4.5 was used with prescribed satellite-based phenology, taken from the Moderate Resolution Imaging Spectroradiometer (MODIS; Lawrence and Chase, 2007).

In this study, CLM4.5 was forced by a 34-yr (1979–2012) observation-based atmospheric forcing dataset from the Institute of Tibetan Plateau Research, Chinese Academy of Sciences (hereafter ITP), with a spatial resolution of 0.1° × 0.1° at a three-hourly temporal resolution over China (15–55 °N, 70–140 °E). This dataset was constructed by merging the observations from 740 operational stations of the CMA with the corresponding meteorological forcing dataset from the Global Land Data Assimilation System (Rodell et al., 2004) to produce near-surface air temperature, pressure, wind speed and specific humidity fields. It combined three precipitation datasets, including ground-based observations and two satellite retrieval products (Chen et al., 2011), to determine the precipitation field. It also corrected the Global Energy and Water Cycle Experiment–Surface Radiation Budget (Pinker and Laszlo, 1992) with reference to radiation estimates (Yang et al., 2010) to ascertain the incident shortwave radiation fields. Chen et al. (2011) demonstrated that simulations driven by the ITP forcing data improve land surface temperature modeling for dry land in China. The soil moisture simulations of CLM3.5, an old version of CLM4.5, forced by four different atmospheric forcing datasets were compared against a common set of in situ observations and results showed that, over most regions of China, the soil moisture estimations forced by the

ITP forcing dataset had closer correlations with ground-based observations than did the three other simulations (Liu and Xie, 2013).

2.2 ESA CCI SM data

In response to the Global Climate Observing System endorsement of soil moisture as an essential climate variable, the ESA-WACMOS and CCI projects have supported the generation of the ESA CCI SM product by merging multiple microwave-based soil moisture products (Wagner et al., 2012), including passive data derived from SMMR, SSM/I, TMI, and AMSR-E and active data from the ERS and ASCAT (Liu et al. 2011, 2012). The ESA CCI SM version 2.0 (v2.0), released by the Vienna University of Technology in July 2014, was used in this study. Compared to previous versions, the merging schemes and procedures for ESA CCI SM v2.0 has been improved. Furthermore, the dataset was extended to the year 2013 by including the WindSat and AMSR2 data (Parinussa et al., 2012, 2015). Initially, the ESA CCI SM data were separated into two homogenized products (one for active and one for passive data); and then merged into a single active-passive product according to their relative sensitivity to vegetation density (Liu et al, 2011, 2012; Wagner et al., 2012). The ESA CCI SM has a spatial resolution of 0.25° × 0.25° (unit: $m^3\ m^{-3}$) and a daily time-step centered at 0:00 UTC, although the actual observation time corresponds to that of the input products at a specific time (Liu et al., 2012). Quality "flags" of the input products were transferred to ESA CCI SM to mask pixels affected by snow coverage, temperature below 0 °C, dense vegetation, and pixels where the retrieval of soil moisture data failed (Dorigo et al., 2015).

2.3 In situ measurements in China

This study made use of in situ soil moisture measurements from agricultural meteorological stations across mainland China, collected by the CMA-NMIC, to evaluate the ESA CCI SM and CLM4.5. The original data for 20 years (1993–2012) from 778 stations were obtained every 10 days (i.e., on the 8th, 18th and 28th day of every month) at soil

depths of 0–10, 10–20, 20–50, 50–70 and 70–100 cm, respectively. No measurements were recorded in frozen soil. Soil water content was measured using the gravimetric technique and originally recorded as mass percentage. It was converted to volumetric soil moisture using field capacity and soil bulk density observations (Liu and Xie, 2013). This soil moisture observation dataset has been widely used to study temporal variations in soil moisture and evaluate land surface model simulations in China (Li et al., 2005; Wang and Zeng, 2011; Liu and Xie, 2013), and is constantly updated. However, not all datasets are suitable for the evaluation of remote sensing products and model simulations. In this study, we used a simple quality control procedure (Wang and Zeng, 2011; Liu and Xie, 2013) on the updated soil moisture observations in terms of observation frequency; specifically, the ratio of valid measurements during the period from March to October (1993–2012) was required to be greater than 50%. It is noted that if more than one in situ station remained in a single 0.25° grid box, only one of them was included. The correlation check method was adopted to remove the redundant sites (Dorigo et al., 2015); in this procedure, the correlation between the in situ measurements and ESA CCI SM product and that between the in situ measurements and CLM4.5 were first calculated, respectively, and their average value was compared for each site, after which the site with the highest average correlation was selected. Finally, the monthly soil water content values at depths of 0–10 cm at 306 stations were used in this study to evaluate the remotely sensed and simulated values. These stations were grouped into eight sub-regions on the basis of the spatial patterns of the centers of dryness and wetness throughout China, based on Zhu (2003) and Liu and Xie (2013), and are defined in Table 1. Figure 1 shows the eight sub-regions and the location of all 306 in situ measurement sites, 289 of which were located in the eight sub-regions in this study.

2.4 Evaluation strategy

For the CLM4.5 simulation, we first spun up 300 years by repeating 30-yr (1979–2009)

ITP meteorological forcing data to achieve an equilibrium state. The 1979–2012 atmospheric forcing data were then used to force CLM4.5 and the simulated results were used in this study. To be consistent with the ESA CCI SM dataset, these simulations were all made at spatial resolution of 0.25° × 0.25° at 30-min time-steps. It should be noted that the data affected by snow cover and temperatures below 0 °C for both the in situ measurements and CLM4.5 predictions between March and October were masked using the quality flags of the ECV CCI SM product. Given the low temporal frequency of the in situ datasets, the validation of the ESA CCI SM and CLM4.5 was conducted at the monthly timescale to reduce the effect caused by the mismatch between actual observation and model time (Wang and Zeng, 2011; Liu and Xie, 2013). Only daily data of the ESA CCI SM product and CLM4.5 simulation on the days of each month when in situ observations were available were used to compute their monthly mean values.

The 'nearest neighbor' approach was retained to match the grid point location from the ESA CCI SM product or CLM4.5 simulation with that of the in situ measurements. Since soil layer thickness of CLM4.5 model did not match that of in situ observations (0−10 cm), the weighted average was computed based on top four soil layer thicknesses (1.75, 2.76, 4.55, 0.94 cm, respectively).

Previous studies (Loew et al., 2013; Dorigo et al., 2015) pointed out that the statistical metrics, e.g., the bias and the root mean square difference (RMSD), principally reflected the differences between the in-situ data and the GLDAS-Noah model dataset that was used as a reference for scaling, and thus were scientifically not meaningful. Besides, at the level of the individual stations little is known about the accuracy of the measurements themselves and the ability of the sites to represent absolute soil moisture levels over the coarse satellite footprint scale (Gruber et al., 2013). Therefore, the unbiased RMSD (ubRMSD) was used to express differences in soil moisture levels in this study, and can be calculated using Eq. (1):

$$\mathrm{ubRMSD} = \sqrt{\frac{1}{n}\sum_{i=1}^{n}\left[(S_i - \overline{S}) - (O_i - \overline{O})\right]^2}, \quad (1)$$

in which S represents soil moisture from either the ESA CCI SM dataset or CLM4.5 simulation, O is the in situ measurement and $\overline{S}$ and $\overline{O}$ are the corresponding mean values related to S and O. It is noted that, prior to computing the ubRSMD, both the ESA CCI SM dataset and CLM4.5 simulations were scaled into the dynamic range of the in situ data using a linear rescaling method based on the mean and standard deviation (Brocca et al., 2013):

$$S_{res} = \frac{S - \overline{S}}{\sigma_S} \times \sigma_O + \overline{O}, \quad (2)$$

where S_{res} is the linearly rescaled soil moisture dataset, and σ_S and σ_O are the corresponding standard deviations related to S and O, respectively. In addition, the Spearman rank correlation (R_{sp}) was calculated to describe the temporal agreement between the in situ data and the ESA CCI SM dataset and CLM4.5 simulation (Dorigo et al., 2015).

Because the different products used to develop ESA CCI SM vary over space and time, the differences in the microwave observation channels and sampling densities are expected to influence the quality of the different periods for evaluating the new merged satellite product (Liu et al., 2012; Dorigo et al., 2015). The following describes the eight sub-periods used to construct the ESA CCI SM dataset (Albergel et al., 2013a; Dorigo et al., 2015):

- blend 1: January 1979–August 1987, based on SMMR observations only;
- blend 2: September 1987–June 1991, based on SSM/I only;
- blend 3: July 1991–December 1997, based on a combination of SSM/I and ERS AMI;
- blend 4: January 1998–June 2002, based on a combination of TMI and AMI between 40 °N and 40 °S, and a combination of SSM/I and ERS AMI elsewhere;
- blend 5: July 2002–December 2006, based on a combination of AMSR-E and ERS AMI;
- blend 6: January 2007–September 2011, based on a combination of AMSR-E and ASCAT;

- blend 7: October 2011–June 2012, based on a combination of WindSat and ASCAT;
- blend 8: July 2012–December 2013, based on a combination of AMSR2 and ASCAT.

To illustrate the potential effects of these developmental stages on the quality of the ESA CCI SM dataset, the product evaluation was repeated for the last five time periods (during which in situ observations were available).

3. Results

3.1 Availability of the ESA CCI SM data in China

Previous studies (Loew et al., 2013; Dorigo et al., 2015) showed that the performance of the ESA CCI SM product may be strongly affected by data gaps and the period of observation. Therefore, we first analyzed the data availability of the ESA CCI SM product in China for the entire period (1979–2013) as well as for the eight individual time periods (described in Section 2.4). A clear increase of observation density can be observed over time (Fig. 2), which is mainly due to the growing number of satellites available for soil moisture data retrieval (Liu et al., 2012; Dorigo et al., 2015). The improved instrument design and sensor performance also contributes to this effect. Better sensors have led to a convergence of active and passive remote sensing products, especially over areas with intermediate vegetation cover (Liu et al., 2012), and an increase over time in the number of areas where both products are used in a synergistic way.

For example, for the second period (1 September 1987–30 June 1991), the ESA CCI SM product was generated using the SSM/I Ku-band (19.3 GHz) data alone, which was strongly attenuated by the vegetation canopy; thus, large areas were masked due to moderate to dense vegetation, such as northeast and southern China (Fig. 2b). The introduction of the ERS AMI C-band (5.3 GHz) scatterometer during the subsequent period (1 July 1991–31 December 1997) was able to partly fill these gaps (Fig. 2c), e.g. there was a clear increase in the number of observations over southern China. With the introduction of the high quality AMSR-E

C-band (6.9 GHz) data in July 2002, a large increase of the observation density can be found over most areas of China, except the Tibetan Plateau (Fig. 2e). As a result of the unavailability of the AMSR-E data in October 2011, the observation density decreased over large parts of northwest China and Inner Mongolia, which are mainly arid or semiarid areas, despite the inclusion of the high quality WindSat data for this period (Fig. 2g). In addition, the introduction of the AMSR2 product clearly increases the fractions of valid observations over most areas of China, except central and southern China (Fig. 2h).

3.2 Evaluation using in situ data

Figure 3 presents the Spearman rank correlation coefficients (R_{sp}) of the ESA CCI SM product and CLM4.5 simulation against in situ measurements, in which the values from both techniques are ranked using the same intervals. The data gaps for the ESA CCI SM product (Fig. 2) lead to only 299 stations available; over 61% of these stations had correlation values between 0.2 and 0.6 (shown in green and purple, Fig. 3a), with a mean of 0.27 (Table 2). In contrast, the CLM4.5 model captured surface soil moisture temporal variability better (averaged R value is 0.35, Table 2) than the ESA CCI SM product; about 10% of the stations had R_{sp} values greater than 0.6 (shown as orange and blue, Fig. 3b), whereas only 5% stations for the ESA CCI SM achieved such correlations (Fig. 3a). When only the configurations associated to significant correlation values ($p < 0.05$) are considered (cycles), there were 212 and 253 stations available for the ESA CCI SM and CLM4.5, respectively. In the current study, the averaged R_{sp} value of the ESA CCI SM is 0.37, which is slightly higher than that ($R_{sp} = 0.32$) from 34 sites over China in Dorigo et al. (2015); the averagd R_{sp} is 0.42 for the CLM4.5 model.

As described in several studies (Liu et al., 2011, 2012; Dorigo et al., 2015), the mean and dynamic range of the ESA CCI SM time series represent those of the GLDAS-Noah surface soil moisture product. Therefore, we used a linear rescaling method (Eq. 2) to rescale

both the ESA CCI SM dataset and CLM4.5 soil moisture predictions prior to computing their ubRMSDs (Brocca et al., 2013) against in situ measurements (Fig. 4). For the ESA CCI SM product, there were 214 stations (72% of total) with the ubRMSD values less than 0.06 m^3 m^{-3}. The CLM4.5 showed a slightly improved ubRMSD, of which about 29% of the stations had a value less than 0.04 m^3 m^{-3} (Fig. 4b), compared to 22% using the ESA CCI SM product (Fig. 4a). Table 2 shows that averaged ubRMSD values are 0.053 and 0.050 m^3 m^{-3} for the ESA CCI SM product and CLM4.5 simulation, respectively, which suggests that the CLM4.5 simulation is closer to in situ measurements in China than is the ESA CCI SM product. When only sites with a significant ($p < 0.05$) positive Spearman's correlation were considered (cycles in Figs. 3 and 4), the averaged ubRMSD values were 0.050 and 0.048 m^3 m^{-3} for the ESA CCI SM product and CLM4.5 simulation, respectively. It should be noted that because the ubRMSD is only an indication of the mismatch between in situ data and remote sensing or model simulated datasets, the errors in each dataset are also included. The triple collocation technique has proven to be an independent technique for estimating the random error component of soil moisture datasets and been applied to the direct comparison with the ubRMSD metric (Dorigo et al., 2010; Gruber et al., 2013; Dorigo et al., 2015). Therefore, future work is expected to use this method to reduce the effect of random errors in each dataset on the comparison.

3.3 Performances over eight sub-regions

Since soil moisture has a close relationship with the status of climate dryness and wetness, eight sub-regions were defined (Table 1 and Fig. 1) in this study based on Zhu (2003), which used a time series for dryness and wetness encompassing the last 530 years to analyze the spatial patterns of the centers of dryness and wetness throughout China by applying the rotated empirical orthogonal function method. To evaluate the performance of the satellite-based product and process-based model simulation over eight sub-regions, two

evaluation strategies were adopted in our study: (1) we computed the statistical metrics for the stations individually (e.g., Figs. 3 and 4) and then averaged their values over each region (hereinafter referred to as "S1"); (2) we generated the time series of soil moisture by averaging available observations at all stations of each region, only considering those grid cells closest to the relevant observation stations for the ESA CCI SM product and CLM4.5 simulation, and then calculated their statistical metrics against in situ measurements (hereinafter referred to as "S2"). It should be noted that only sites with a significant ($p < 0.05$) positive Spearman's correlation (cycles in Figs. 3 and 4) for both ESA CCI SM product and CLM4.5 simulation were considered in the following analysis whatever the evaluation strategy. After screening using the criteria above, 200 stations remained available for the following evaluation, 189 of which were located in the eight sub-regions; the number of valid stations for each sub-region is shown in Table 2 (in the brackets). The statistical metrics of the ESA CCI SM product and CLM4.5 simulation against in situ measurements for both evaluation strategies are presented in Fig. 5.

Over most regions (except for China V), the ESA CCI SM product, of which average ubRMSD values ranged between 0.044 and 0.059 $m^3\ m^{-3}$, had slightly higher ubRMSD values than CLM4.5 simulations (0.042−0.056 $m^3\ m^{-3}$) for the first evaluation strategy (Fig. 5a), which is consistent with the results from Fig. 4 and Table 2. Figure 5b shows that the average Spearman correlation coefficients of the ESA CCI SM product ranged between 0.27 and 0.47, while higher correlations in situ measurements were achieved by CLM4.5 simulations (0.34–0.54), except in China V. Good performance over China V, which is a semi-arid region, for the ESA CCI SM product was also found by Albergel et al. (2013b) and Dorigo et al., (2015) using in situ observations from the Maqu network, which is located over the southern part of this sub-region. Our finding suggests that the ESA CCI SM product has a good potential for application in areas where models cannot realistically represent soil

moisture (Albergel et al., 2013b).

Compared to S1, the other strategy (S2) showed large variations in ubRMSD (Fig. 5a) and R_{sp} (Fig. 5b) between different sub-regions. However, the two strategies produced similar results although CLM4.5 simulations showed a slightly higher R_{sp} and lower ubRMSD than the ESA CCI SM product. In addition, compared with performance in other regions, both remotely sensed and modeled soil moisture datasets showed larger ubRMSD values over southwest China (China VII and VIII), which is mainly covered with moderate to dense vegetation, including mixed evergreen coniferous and broadleaf deciduous forests, and broadleaf deciduous forests. This result is mainly due to strong attenuation by the vegetation canopy of the microwave retrievals for the ESA CCI SM product (Liu et al., 2012; Dorigo et al., 2015). For the CLM4.5 simulation, the precipitation data in the ITP atmospheric forcing data were generated by merging ground-based observations and two satellite retrieval products, because few in situ precipitation measurements were available over these areas (Chen et al., 2011).

Figure 6 compares the annual soil moisture cycle (March−October) of the ESA CCI SM product and CLM4.5 simulation against in situ measurements, averaged over the eight sub-regions using the S2 evaluation strategy (without the linear scaling). Both the ESA CCI SM product and CLM4.5 simulation generally captured the annual cycle well in most sub-regions. However, soil moisture simulated by the CLM4.5 model was usually greater than the observations, showing systematic overestimation in all sub-regions except for China VI and VIII; this is consistent with the research of Liu and Xie (2013), which was based on simulations with the CLM3.5 model using the same atmospheric forcing data as we used. The comparable findings suggest that land surface model simulation may reproduce temporal variations well, but fail to simulate the mean soil moisture (Entin et al., 2000; Gao and Dirmeyer, 2006; Liu and Xie, 2013). In contrast, the ESA CCI SM product was closer to

matching in situ measurements than the CLM4.5 model over some areas (e.g., China V in this study, a semi-arid region), although it represents the dynamic range of the GLDAS-Noah surface soil moisture product (Liu et al., 2012; Dorigo et al., 2015).

3.4 Comparison of the anomaly time series

The results presented above are based on comparisons of the multi-year observation dataset and the ESA CCI SM or CLM4.5 datasets on a monthly timescale, which may be somewhat affected by the seasonal cycle of soil moisture. The time series of the soil moisture anomaly from the three datasets (ESA CCI SM, CLM4.5, and in situ observations) for the eight sub-regions using the S2 strategy (Section 3.3), computed by removing the multi-year annual cycle (only March−October available), are presented in Fig. 7. In general, both the ESA CCI SM product and the CLM4.5 simulation captured the temporal evolution of the observed soil moisture anomalies reasonably well for most of the regions, except a slight overestimation in the amplitude of fluctuations over China VII and VIII by the ESA CCI SM product, which was consistent with the results shown in Fig. 5.

As a further quantitative illustration of the effects of seasonal cycle on the evaluation results, Fig. 8 shows the Spearman correlation coefficients (R'_{sp}) for the anomaly data of both the ESA CCI SM product and CLM4.5 simulation over the eight sub-regions. In general, R'_{sp} values (Fig. 8) were lower than R_{sp} (Fig. 5) for most sub-regions, especially over China VI and VIII. This differences suggested that the seasonal cycle in soil moisture has a large effect on the comparison of Spearman correlation values over the areas with pronounced wet and dry periods (Liu et al., 2012; Albergel et al., 2013a; Dorigo et al., 2015).

3.5 Evolution of the ESA CCI SM over time

The microwave observation channels and sampling densities were expected to affect the quality of the dataset for different periods because the different products that were used to generate the ESA CCI SM dataset vary over space and time (Liu et al., 2012; Albergel et al.,

2013a). Figure 9 presents the averaged ubRMSDs and R_{sp} of the ESA CCI SM product for the last five individual time periods defined in Section 2.4. Due to limited time length and sparse samples for the last two blended periods (blend 7 and blend 8), they were combined into one period. Considering the sites that have significant R_{sp} values ($p = 0.05$) for all periods (denoted by red in Fig. 9), averaged correlations ranged from 0.42 to 0.62 while ubRMSD values ranged from 0.024 $m^3\ m^{-3}$ to 0.045 $m^3\ m^{-3}$. A similar pattern was obtained when considering the sites for which the correlation was significant for each blended period with averaged R_{sp} values ranging from 0.56 to 0.93.

For the fourth period (January 1998–June 2002), a higher correlation was observed (Fig. 9b) compared to the previous period (January 1993–December 1997), which may be related to the introduction of the circular non-polar orbiting TMI data in 1998 (Doirgo et al., 2015). In July 2002, a high quality soil moisture dataset from C-band AMSR-E retrievals was introduced instead of the SSM/I and TMI, which increased the correlations of the ESA CCI SM dataset with in situ measurements and reduced its ubRMSD values for the fifth period (July 2002–December 2006). These observations were consistent with the results of the comparison between the ESA CCI SM and the ERA-Land, an update of the land surface component of the ERA-Interim reanalysis from the European Centre for Medium-Range Weather Forecasts (Albergel et al. 2013a), and that between the ESAI CCI SM product and in situ measurements from other soil moisture networks (Dorigo et al., 2015). Unexpectedly, there was a decrease in quality in the sixth period (January 2007–September 2011), with weaker correlations and higher ubRMSD (Albergel et al., 2013a, Dorigo et al., 2015). The cause of this degradation is still not entirely clear, but it may be related to the resampling and scaling strategy used to incorporate a new active input product from ASCAT (Dorigo et al., 2015). The best performance for all metrics was obtained for the last two periods (October 2011–December 2012), which was expected, given the higher quality satellite

instrumentation (AMSR2) and improved retrieval algorithms. However, the shorter length of time within the two periods may have had a slight effect on the statistical metrics and therefore more in situ measurements would be needed to confirm our results.

4. Discussion

During the past twenty years, huge efforts have been made to make more in situ soil moisture observations available in China. These measurements are important for the evaluation of both remotely sensed and modeled soil moisture. In this study, we evaluated the performances of the ESA CCI SM product and CLM4.5 simulation in China using 20 years of in situ observations from 306 sites. However, some limitations to the evaluation should be noted. The spatial representativity, temporal mismatch, instrumental errors, and installation depth of in situ observations may have had a negative effect on the evaluation results. Such limitations have been extensively reported in previous studies (Brocca et al., 2010; Crow et al., 2012). Therefore, future work is expected to reduce these uncertainties through the enhancement of ground-based measurements and the improvement of the evaluation strategy. In addition, soil moisture was measured using the gravimetric technique. This destructive sampling method may affect the evaluation results (Dorigo et al., 2015). According to the user guide of in situ soil moisture measurements from agricultural meteorological stations of CMA (in Chinese, http://cdc.nmic.cn), soil moisture observation technique can be summarized as follows: (1) the observation field of each station is divided to four parts and four soil samples will be collected each time; (2) their soil moisture contents in dry weight basis (the ratio of water mass to dried soil's weight) are determined by drying the soil, respectively; (3) the average value from the four samples are recorded as mass percentage for this station. It is noted that the horizontal distance between two successive samples at the same part of each station is no more than 2 meters, which leads to almost the same meteorological and soil conditions. Moreover, to reduce the effect of soil moisture

heterogeneity, the station was usually chosen to be over flat surface. However, the original observations from the four samples at each station were not available; thus, we could not investigate the effect of destructive sampling on the comparison results in this study. Previous studies (Brocca et al., 2014a, b) showed that soil moisture had enormous variability even at local scales, in particular in absolute terms. These methods will be used in our future work to discuss the impacts of spatial variability and destructive sampling method.

Land surface models can capture the temporal dynamics of soil moisture well when forced by high quality atmospheric forcing data (Albergel et al., 2010, 2012) and are usually employed to upscale in situ surface soil moisture observations or complete the evaluation of satellite derived products (Albergel et al., 2013a). In this study, the CLM4.5 was forced by an atmospheric forcing dataset generated using many ground-based observations, and showed better correlation with in situ soil moisture observations than did the ESA CCI SM product. However, many precipitation measurements were located in the same 0.25° grid box as the in situ soil moisture observations; although the two types of data were obtained from different sources and were not collected at the same locations, it was necessary to investigate the effect of in situ precipitation measurements on the comparison results. The averaged statistical metrics over the sites with ("Rain") and without ("No Rain") in situ precipitation measurements are presented in Fig. 10. It is noted that only the sites (200 of 306) with a significant ($p < 0.05$) positive Spearman's correlation for both the ESA CCI SM product and CLM4.5 simulation were considered, as described in Section 3.2. Figure 10 shows that, for the CLM4.5 simulation, in situ precipitation measurements (101 of 200) led to a slightly higher correlation ($R_{sp} = 0.46$) with in situ soil moisture measurements than was obtained without the precipitation measurements ($R_{sp} = 0.44$, 99 of 200). This may be related to the issues of spatial resolution. The observations from 740 operational stations of the CMA were merged with other meteorological forcing datasets to generate the ITP forcing data with a

spatial resolution of 0.1° × 0.1°, while the CLM4.5 was run at 0.25° × 0.25° resolution in this study. If the CLM4.5 had been run at 0.1° × 0.1° resolution, the effect of ground-based precipitation on the comparison results may have been clearer (not shown in this study).

The in situ observations used in this study are average soil moisture values of surface soil of 0−10 cm; to be consistent with the in situ observations, the weighted average of CLM4.5 at 0−10 cm was computed based on the uppermost four soil layer thicknesses (Section 2.4). However, the ESA CCI SM data represent the upper 0−2 cm of the soil (Liu et al., 2011, 2012; Dorigo et al., 2015). As in situ soil moisture observations of 0−2 cm are not available, it is difficult to investigate the effect of the mismatch between soil depths on the statistical results. Instead, we compared the in situ observations and ESA CCI SM data with average soil moisture values of CLM4.5 at different soil depths: first layer ("L1", 0−1.75 cm), uppermost two layers ("L1−2", 0−1.75 cm, 1.75−4.51 cm), uppermost three layers ("L1−2−3", 0−1.75 cm, 1.75−4.51 cm, 4.51−9.06 cm), 0−2 cm, 0−5 cm, and 0−10 cm. Their statistical metrics, including ubRMSD and R_{sp}, are presented in Fig. 11. Results showed that the choice of soil depth for CLM4.5 had a significant effect on the statics. The average R_{sp} against in situ observations ranged between 0.417 and 0.425 at different soil depths while the ESA CCI SM had higher R_{sp} values and a larger range, which was between 0.507 and 0.546. CLM4.5 agreed better with in situ observations at 0−10 cm than those at other soil depths, confirming that it is better to evaluate the CLM4.5 using the weighted average values at 0−10 cm. In contrast, the best agreement between the CLM4.5 simulation and ESA CCI SM product was found at the first layer (0−1.75 cm). These findings suggest that the mismatch in soil depths between the ESA CCI SM and in situ observations may have had a large effect on the statistical metrics, which is one of the reasons for its higher ubRMSD and lower R_{sp}.

In addition, although the CLM4.5 model had better performance against in situ observations than the ESA CCI SM product over most regions in China, there were still many

unrealistic representations in model parameterizations (soil water and temperature, for example) and large uncertainties in land surface datasets (such as soil texture and PFTs) for the CLM4.5 model, which affected its accuracy in soil moisture simulation. To improve soil moisture estimations, many studies have incorporated remotely sensed brightness temperatures (Jia et al., 2013) or soil moisture retrievals (Draper et al., 2012) into land surface models using various modern land data assimilation systems. Our study provides an in-depth evaluation of both the ESA CCI SM product and CLM4.5 model in China, including their performances over different sub-regions. This evaluation is expected to be useful for the assimilation of the ESA CCI SM product into land surface models, especially the CLM4.5, because the observation and model errors have been estimated approximately.

For the ESA CCI SM product, only soil moisture retrievals acquired by night time overpasses (occurring between 19:00 and 08:00 local time) were used (Liu et al., 2012) because all input products had varying local observation times (Dorigo et al., 2015). However, the original in situ soil moisture observations were available every 10 days (three times each month) and the time step of CLM4.5 was 30 min. To reduce the effect caused by the mismatch between actual observation and model time, we compared the three datasets at a coarser time scale using their monthly values, in a similar way as previous studies (Li et al., 2005; Wang and Zeng, 2011; Liu and Xie, 2013). However, it should be noted that the effect of the temporal mismatch among different soil moisture datasets was not considered in this study.

5. Conclusions

In this study, the performances of a microwave-based merged satellite product (ESA CCI SM) and the CLM4.5 simulation were investigated using 20 years of in situ observations from 306 stations in China. In general, both soil moisture products represent in situ observations well, with ubRMSD values of about 0.05 $m^3 m^{-3}$. The ESA CCI SM product has

525 slightly weaker Spearman correlations (R_{sp} = 0.37) than the CLM4.5 model, but the CLM4.5
526 simulation produces better temporal variation of surface soil moisture (R_{sp} = 0.42).

527 Both the satellite product and model simulation show large discrepancies over eight
528 sub-regions in China. The CLM4.5 model shows larger ubRMSDs in southwestern China
529 (China VII and VIII) than other regions, which may be related to the scarcity of in situ
530 precipitation measurements available in these areas. The ESA CCI SM product is likely to be
531 best-suited for applicaiton in semi-arid regions (such as China V), even better than the
532 CLM4.5 model, mainly because of accurate data retrievals and high observation density; in
533 contrast, the ESA CCI SM product is not well suited for areas covered by dense vegetation
534 (such as China VII and VIII). In addition, the statistical scores of the ESA CCI SM product in
535 China corroborate the findings of Albergel et al. (2013a) and Dorigo et al. (2015) of a stable
536 to slightly improving performance over time in China, with the exception of a decrease
537 during the 2007–2010 blending period, which may be related to the resampling and scaling
538 strategy used to incorporate the ASCAT product into the ESA CC SM dataset.

539 In response to the sparse observation temporal frequency (three times each month), all
540 analyses were performed on a monthly timescale. Future efforts are expected to make more in
541 situ soil moisture observations available in China for the evaluation of either remote sensing
542 retrievals or modeled simulation. Furthermore, data assimilation has been an effective tool to
543 incorporate remotely sensed soil moisture into land surface models to improve soil moisture
544 simulation (Draper et al., 2012). The in-depth evaluation of the ESA CCI SM product and
545 CLM4.5 model in China provided by this study will facilitate soil moisture data assimilation,
546 which is expected to provide further information regarding observation and model errors.
547

548 ***Acknowledgements***

549 This research was supported by the National Natural Science Foundation of China (Grant

Numbers: 41305066, 41405083 and 91125016), the Special Funds for Public Welfare of China (Grant Number: GYHY201306045) and the Natural Science Foundation of Hunan Province (Grant Number: 2015JJ3098). The ESA soil moisture dataset was downloaded from http://www.esa-soilmoisture-cci.org; the in situ soil moisture observations were downloaded from http://cdc.nmic.cn/. The forcing dataset used in this study was developed by the Data Assimilation and Modeling Center for Tibetan Multi-spheres, Institute of Tibetan Plateau Research, Chinese Academy of Sciences. We also thank the editor, Prof. Alexander Loew, the reviewer, Dr. Wouter Dorigo, and another anonymous reviewer for their constructive comments and suggestions, which have significantly improved our paper.

559 # References

560 Albergel, C., de Rosnay, P., Gruhier, C., Muñoz-Sabater, J., Hasenauer, S., Isaksen, L., Kerr,
561 Y., and Wagner, W.: Evaluation of remotely sensed and modelled soil moisture products
562 using global ground-based in situ observations, Remote Sens. Environ., 118, 215–226,
563 2012.

564 Albergel, C., Dorigo, W., Balsamo, G., Muñoz-Sabater, J., de Rosnay, P., Isaksen, L., Brocca,
565 L., de Jeu, R., and Wagner, W.: Monitoring multi-decadal satellite earth observation of
566 soil moisture products through land surface reanalyses, Remote Sens. Environ., 138,
567 77–89, 2013a.

568 Albergel, C., Dorigo, W., Reichle, R., Balsamo, G., de Rosnay, P., Muñoz-Sabater, J.,
569 Isaksen, L., and Wagner, W.: Skill and global trend analysis of soilmoisture
570 fromreanalyses andmicrowave remote sensing, J. Hydrometeor., 14, 1259–1277, doi:
571 10.1175/JHM-D-12-0161.1, 2013b.

572 Albergel, C., Rudiger, C., Carrer, D., Calvet, J. C., Fritz, N., Naeimi, V., Bartalis, Z., and
573 Hasenauer, S.: An evaluation of ASCAT surface soil moisture products with in-situ
574 observations in Southwestern France, Hydrol. Earth Syst. Sci., 13, 115–124, 2009.

575 Bartalis, Z., Wagner, W., Naeimi, V., Hasenauer, S., Scipal, K., Bonekamp, H., Figa, J., and
576 Anderson, C.: Initial soil moisture retrievals from the METOP-A advanced scatterometer
577 (ASCAT), Geophys. Res. Lett., 34, L20401, doi:10.1029/2007GL031088, 2007.

578 Brocca, L., Ciabatta, L., Massari, C., Moramarco, T., Hahn, S., Hasenauer, S., Kidd, R.,
579 Dorigo, W., Wagner, W., and Levizzani, V. : Soil as a natural rain gauge: Estimating
580 global rainfall from satellite soil moisture data. J. Geophys. Res. Atmos., 119, 5128−5141,
581 doi:10.1002/2014JD021489, 2014a.

582 Brocca, L., Hasenauer, S., Lacava, T., Melone, F., Moramarco, T., Wagner, W., Dorigo, W.,
583 Matgen, P., Martínez-Fernández, J., Llorens, P., Latron, J., Martin, C., and Bittelli, M.:

584 Soil moisture estimation through ASCAT and AMSR-E: An intercomparison and
585 validation study across Europe, Remote Sens. Environ., 115(12), 3390–3408, doi:
586 10.1016/j.rse.2011.08.003, 2011.
587 Brocca, L., Melone, F., Moramarco, T., and Morbidelli, R.: Spatial–temporal variability of
588 soil moisture and its estimation across scales, Water Resour. Res., 46, W02516,
589 doi:10.1029/2009WR008016, 2010.
590 Brocca, L., Zucco, G., Mittelbach, H., Moramarco, T., and Seneviratne, S. I.: Absolute versus
591 temporal anomaly and percent of saturation soil moisture spatial variability for six
592 networks worldwide, Water Resour. Res., 50, 5560–5576, doi:10.1002/2014WR015684,
593 2014b.
594 Brocca, L., Melone, F., Moramarco, T.,Wagner, W., and Albergel, C.: Chapter 17: Scaling
595 and filtering approaches for the use of satellite soil moisture observations. In G. P.
596 Petropoulos (Ed.), Remote sensing of land surface turbulent fluxes and soil surface
597 moisture content: State of the art (pp. 562), Taylor & Francis, 2013.
598 Chen, Y., Yang, K., He, J., Qin, J., Shi, J., Du, J., and He, Q.: Improving land surface
599 temperature modeling for dryland of China, J. Geophys. Res., 116, D20104,
600 doi:10.1029/2011JD015921, 2011.
601 Ciais, P., Reichstein, M., Viovy, N., Granier, A., Ogee, J., Allard, V., Aubinet, M.,
602 Buchmann, N., Bernhofer, C., Carrara, A., Chevallier, F., De Noblet, N., Friend, A. D.,
603 Friedlingstein, P., Grunwald, T., Heinesch, B., Keronen, P., Knohl, A., Krinner, G.,
604 Loustau, D., Manca, G., Matteucci, G., Miglietta, F., Ourcival, J. M., Papale, D.,
605 Pilegaard, K., Rambal, S., Seufert, G., Soussana, J. F., Sanz, M. J., Schulze, E. D., Vesala,
606 T., and Valentini, R.: Europe-wide reduction in primary productivity caused by the heat
607 and drought in 2003, Nature, 437, 529–533, doi:10.1038/nature03972, 2005.
608 Crow, W. T., Berg, A. A., Cosh, M. H., Loew, A., Mohanty, B. P., Panciera, R., de Rosnay,

609 P., Ryu, D., and Walker, J. P.: Upscaling sparse ground-based soil moisture observations
610 for the validation of coarse-resolution satellite soil moisture products, Rev. Geophys., 50,
611 RG2002, doi:10.1029/2011RG000372, 2012.
612 de Rosnay P., Drusch, M., Vasiljevic, D., Balsamo, G., Albergel, C., and Isaksen, L.: A
613 simplified Extended Kalman Filter for the global operational soil moisture analysis at
614 ECMWF, Q. J. R. Meteorol. Soc., 139(674), 1199–1213, doi: 10.1002/qj.2023, 2013.
615 Dai, A., Trenberth, K. E., and Qian, T. T.: A global dataset of Palmer Drought Severity Index
616 for 1870–2002: Relationship with soil moisture and effects of surface warming, J.
617 Hydrometeor., 5, 1117–1130, doi:10.1175/JHM–386.1, 2004.
618 Dharssi, I., Bovis, K. J., Macpherson, B., and Jones, C. P.: Operational assimilation of
619 ASCAT surface soil wetness at the Met Office, Hydrol. Earth Syst. Sci., 15, 2729–2746,
620 2011.
621 Dirmeyer, P. A., Gao, X., Zhao, M., Gao, Z., Oki, T., and Hanasaki, N.: GSWP-2:
622 Multimodel analysis and implications for our perception of the land surface, Bull. Amer.
623 Meteor. Soc., 87, 1381–1397, 2006.
624 Dorigo, W., de Jeu, R., Chung, D., Parinussa, R., Liu, Y., Wagner, W., and Fernandez, D.:
625 Evaluating global trends (1988–2010) in homogenized remotely sensed surface soil
626 moisture, Geophys. Res. Lett., 39, L18405, doi: 10.1029/2012GL052988, 2012.
627 Dorigo, W. A., Gruber, A., De Jeu, R. A. M., Wagner, W., Stacke, T., Loew, A., Albergel, C.,
628 Brocca, L., Chung, D., Parinussa, R. M., and Kidd, R.: Evaluation of the ESA CCI soil
629 moisture product using ground-based observations, Remote Sens. Environ., 162, 380–395,
630 2015.
631 Dorigo, W. A., Scipal, K., Parinussa, R. M., Liu, Y. Y., Wagner, W., de Jeu, R. A.M., and
632 Naeimi, V.: Error characterisation of global active and passive microwave soil moisture
633 data sets, Hydrol. Earth Syst. Sci., 14, 2605–2616, 2010.

634 Draper, C. S., Walker, J. P., Steinle, P. J., de Jeu, R. A. M., and Holmes, T. R. H.: An
635 evaluation of AMSR-E derived soil moisture over Australia, Remote Sens. Environ., 113,
636 703–710, 2009.
637 Entin, J. K., Robock, A., Vinnikov, K. Y., Hollinger, S., Liu, E. S., and Namkhai, A.:
638 Temporal and spatial scales of observed soil moisture variations in the extratropics, J.
639 Geophys. Res., 105, 11865–11877, 2000.
640 Gao, H., Wood, E. F., Jackson, T. J., Drusch, M., and Bindlish, R.: Using TRMM/TMI to
641 retrieve surface soil moisture over the southern United States from 1998 to 2002, J.
642 Hydrometeor., 7, 23–38, 2006.
643 Gao, X., and Dirmeyer, P. A.: A multimodel analysis, validation and transferability study of
644 global soil wetness products, J. Hydrometeor., 7, 1218–1236, 2006.
645 Gruber, A., Dorigo, W. A., Zwieback, S., Xaver, A. and Wagner, W.: Characterizing
646 coarse-scale representativeness of in-situ soil moisture measurements from the
647 International Soil Moisture Network, Vadose Zone J., 12 (2), doi:10.2136/vzj2012.0170,
648 2013.
649 Gruhier, C., de Rosnay, P., Hasenauer, S., Holmes, T., de Jeu, R., Kerr, Y., Mougin, E.,
650 Njoku, E., Timouk, F., Wagner, W., and Zribi, M.: Soil moisture active and passive
651 microwave products: Intercomparison and evaluation over a Sahelian site, Hydrol. Earth
652 Syst. Sci., 14, 141–156, 2010.
653 Jackson, T. J., and Hsu, A. Y.: Soil moisture and TRMM microwave imager relationships in
654 the Southern Great Plains 1999 (SGP99) experiment, IEEE Trans. Geosci. Remote Sens.,
655 39, 1632–1642, 2001.
656 Jia, B., Tian, X., Xie, Z., Liu, J., and Shi, C.: Assimilation of microwave brightness
657 temperature in a land data assimilation system with multi-observation operators, J.
658 Geophys. Res., 118, doi:10.1002/jgrd.50377, 2013.

659 Kerr, Y. H., Waldteufel, P., Richaume, P., Wigneron, J. P., Ferrazzoli, P., Mahmoodi, A., Al
660 Bitar, A., Cabot, F., Gruhier, C., Juglea, S. E., Leroux, D., Mialon, A., and Delwart, S.:
661 The SMOS soil moisture retrieval algorithm, IEEE Trans. Geosci. Remote Sens., 50,
662 1384–1403, 2012.
663 Lai, X., Wen, J., Cen, S., Huang, X., Tian, H., and Shi, X.: Spatial and temporal soil moisture
664 variations over China from simulations and observations, Adv. Meteorol., 2015, 529825,
665 2015.
666 Lawrence, P. J., and Chase, T. N.: Representing a new MODIS consistent land surface in the
667 Community Land Model (CLM 3.0), J. Geophys. Res., 112, G01023,
668 doi:10.1029/2006JG000168, 2007.
669 Li, H. B., Robock, A., Liu, S. X., Mo, X. G., and Viterbo, P.: Evaluation of reanalysis soil
670 moisture simulations using updated Chinese soil moisture observations, J. Hydrometeor.,
671 6, 180–193, 2005.
672 Liu, J. G., and Xie, Z. H.: Improving simulation of soil moisture in China using a multiple
673 meteorological forcing ensemble approach, Hydrol. Earth Syst. Sci., 17, 3355–3369,
674 doi:10.5194/hess-17-3355-2013, 2013.
675 Liu, Y. Y., Dorigo, W. A., Parinussa, R., de Jeu, R. A. M., Wagner, W., McCabe, M. F.,
676 Evans, J. P., and van Dijk, A. I. J. M.: Trend-preserving blending of passive and active
677 microwave soil moisture retrievals, Remote Sens. Environ., 123, 280–297, 2012.
678 Liu, Y. Y., Parinussa, R., Dorigo, W. A., De Jeu, R. A.M., Wagner, W., van Dijk, A. I. J. M.,
679 McCabe, M. F., and Evans, J. P.: Developing an improved soil moisture dataset by
680 blending passive and active microwave satellite-based retrievals, Hydrol. Earth Syst. Sci.,
681 15, 425–436, doi:10.5194/hess-15-425-2011, 2011.
682 Loew, A., Stacke, T., Dorigo, W., de Jeu, R., and Hagemann, S.: Potential and limitations of
683 multidecadal satellite soil moisture observations for selected climate model evaluation

684 studies, Hydrol. Earth Syst. Sci., 17, 3523–3542, 2013.
685 Njoku, E. G., Jackson, T. L., Lakshmi, V., Chan, T., and Nghiem, S. V.: Soil moisture
686 retrieval from AMSR-E, IEEE Trans. Geosci. Remote Sens., 41, 215–229, 2003.
687 Oleson, K. W., Lawrence, D. M., Bonan, G. B., Drewniak, B., Huang, M., Koven, C. D.,
688 Levis, S., Li, F., Riley, W. J., Subin, Z. M., Swenson, S. C., Thornton, P. E., Bozbiyik, A.,
689 Fisher, R., Kluzek, E., Lamarque, J.-F., Lawrence, P. J., Leung, L. R., Lipscomb, W.,
690 Muszala, S., Ricciuto, D. M., Sacks, W., Sun, Y., Tang, J., and Yang, Z.-L.: Technical
691 description of version 4.5 of the community land model (CLM), NCAR Technical Note
692 NCAR/TN-503+STR, National Center for Atmospheric Research, Boulder, CO, 420pp,
693 2013.
694 Owe, M., de Jeu, R., and Holmes, T.: Multisensor historical climatology of satellite-derived
695 global land surface moisture, J. Geophys. Res., 113, F01002, doi:10.1029/2007JF000769,
696 2008.
697 Parinussa, R. M., Holmes, T. R. H., and de Jeu, R. A. M.: Soil moisture retrievals from the
698 WindSat polarimetric microwave radiometer. IEEE T. Geosci. Remote Sens., 50,
699 2683−2694, doi:10.1109/TGRS.2011.2174643, 2012.
700 Parinussa, R., Holmes, T., Wanders, N., Dorigo, W., and de Jeu, R.: A preliminary study
701 toward consistent soil moisture from AMSR2, J. Hydrometeor., 16, 932−947,
702 doi:10.1175/JHM-D-13-0200.1, 2015.
703 Pinker, R. T., and Laszlo, I.: Modeling surface solar irradiance for satellite applications on a
704 global scale, Journal of Applied Meteorology, 31, 194–211, 1992.
705 Rodell, M., Houser, P. R., Jambor, U., Gottschalck, J., Mitchell, K., Meng, C. J., Arsenault,
706 K., Cosgrove, B., Radakovich, J., Bosilovich, M., Entin, J. K., Walker, J. P., Lohmann, D.,
707 and Toll, D.: The Global Land Data Assimilation System, Bull. Amer. Meteor. Soc., 85,
708 381–394, 2004.

709 Schmugge, T. J.: Remote sensing of soil moisture: recent advances, IEEE T. Geosci. Remote
710 Sens., 21, 336–344, 1983.
711 Scipal, K.,Wagner,W., Trommler, M., and Naumann, K.: The global soil moisture archive
712 1992–2000 from ERS scatterometer data: first results, in: Proceedings of the IEEE
713 International Geoscience and Remote Sensing Symposium (IGARSS), 24−26 June,
714 Toronto, Canada, 3, 1399−1401, 2002.
715 Szczypta, C., Calvet, J. C., Maignan, F., Dorigo, W., Baret, F., and Ciais, P.: Suitability of
716 modelled and remotely sensed essential climate variables for monitoring
717 Euro-Mediterranean droughts, Geoscientific Model Development, 7, 931–946, 2014.
718 Taylor, K. E.: Summarizing multiple aspects of model performance in a single diagram, J.
719 Geophys. Res., 106, 7183-7192, 2001.
720 Wagner, W., Dorigo, W., de Jeu, R., Fernandez, D., Benveniste, J., Haas, E., and Ertl, M.:
721 Fusion of active and passive microwave observations to create an Essential Climate
722 Variable data record on soil moisture, ISPRS Annals of the Photogrammetry, Remote
723 Sensing and Spatial Information Sciences (ISPRS Annals), Volume I-7, XXII ISPRS
724 Congress, Melbourne, Australia, 25 August–1 September 2012, 315–321, 2012.
725 Wang, A., Lettenmaier, D. P., and Sheffield, J.: Soil moisture drought in China, 1950–2006, J.
726 Climate, 24, 3257–3271, doi: 10.1175/2011JCLI3733.1, 2011.
727 Wang, A., and Zeng, X.: Sensitivities of terrestrial water cycle simulations to the variations
728 of precipitation and air temperature in China, J. Geophys. Res., 116, D02107,
729 doi:10.1029/2010JD014659, 2011.
730 Yang, K., He, J., Tang, W. J., Qin, J., and Cheng, C. C. K.: On downward shortwave and
731 longwave radiations over high altitude regions: Observation and modeling in the Tibetan
732 Plateau, Agr. Forest Meteorol., 150, 38–46, 2010.
733 Zhu, Y. F.: The regional division of dryness/wetness over Eastern China and variations of

734 dryness/wetness in Northern China during the last 530 years (in Chinese), Acta Geogr.
735 Sin., 58, supplement, 100–107, 2003.
736

737 **Table 1.** Locations of the eight sub-regions in China.

Identification	Region Name	Location	Number of Observational Stations
China I	northeast China	120–135 °E, 40–50 °N	61 (40)
China II	northern North China	110–120 °E, 40–45 °N	15 (5)
China III	southern North China	110–120 °E, 34–40 °N	57 (47)
China IV	central and lower Yangtze River Basin	110–122 °E, 30–34 °N	28 (18)
China V	eastern northwest China	95–110 °E, 34–42 °N	77 (53)
China VI	western northwest China	80–95 °E, 34–50 °N	20 (8)
China VII	northern southwest China	100–110 °E, 28–34 °N	22 (12)
China VIII	southern southwest China	100–110 °E, 20–28 °N	9 (6)

738 [a]The values in the brackets represent the number of sites having significant ($p < 0.05$)
739 positive Spearman's correlations for both the ESA CCI SM product and CLM4.5 simulation.
740

741 **Table 2.** Averaged performance metrics and standard deviations of the ESA CCI SM product
742 and CLM4.5 model for all available in situ sites. (Stations: Number of stations; N: Averaged
743 value of number of valid measurements per station; ubRMSD: unbiased root mean square
744 difference; R_{sp}: Spearman correlation coefficient).

	ESA CCI SM	CLM4.5
Stations	299 (212)[a]	306 (253)
N	124 (127)	126 (128)
ubRMSD (m^3 m^{-3})	0.053±0.017 (0.050±0.014)	0.050±0.017 (0.048±0.015)
R_{sp}	0.27 ± 0.21 (0.37 ± 0.14)	0.35 ± 0.21 (0.42 ± 0.14)

745 [a]The values in the brackets represent the average values from the sites having significant ($p <$
746 0.05) positive Spearman correlations.

747

748 **Figures**

749 **Fig. 1** Locations of the 306 in situ soil moisture measurement sites (red dots) in China. Also
750 shown (blue boxes) are the eight sub-regions defined in Table 1.

751 **Fig. 2** Fraction of days with valid observations, expressed as the number of days with
752 observations divided by the total number of days per period, split into six different merging
753 periods: (a) 1 January 1979–31 August 1987, (b) 1 September 1987–30 June 1991, (c) 1 July
754 1991–31 December 1997, (d) 1 January 1998–30 June 2002, (e) 1 July 2002–31 December
755 2006, (f) 1 January 2007–30 September 2011, (g) 1 October 2011–30 June 2012, (h) 1 July
756 2012–31 December 2013; and (i) for the total period 1 January 1979–31 December 2013.

757 **Fig. 3** Spearman rank correlation coefficients (R_{sp}) between the in situ measurements and (a)
758 ESA CCI SM and (b) CLM4.5 from 1993 to 2012 at 306 sites in China. Open circles
759 represent statistically significant Spearman correlation ($p < 0.05$) while closed circles are not
760 significant.

761 **Fig. 4** Unbiased root mean square differences (ubRMSDs) between the in situ measurements
762 and (a) ESA CCI SM and (b) CLM4.5 from 1993 to 2012 at 306 sites in China.

763 **Fig. 5** Statistical scores, including ubRMSD (5a and 5c) and R_{sp} (5b and 5d), for the ESA
764 CCI SM product (red) and CLM4.5 model (blue) between 1993 and 2012 in the eight studied
765 sub-regions of China using two evaluation strategies (S1 and S2). S1: average values of
766 statistical metrics for the stations over each region. S2: statistical metrics with in situ
767 observations for the soil moisture time series averaged at the stations of each region.

768 **Fig. 6** Multi-year (1993–2012) mean monthly volumetric soil moisture (SM, $m^3\ m^{-3}$) for the
769 period between March and October as described by in situ observations, the ESA CCI SM
770 product, and CLM4.5 simulation in the eight studied sub-regions of China.

771 **Fig. 7** Comparison of the anomaly time series of monthly soil moisture derived from the ESA
772 CCI SM product, CLM4.5 simulation, and in situ observations between 1993 and 2012 for

773 the eight studied sub-regions of China.

774 **Fig. 8** Spearman correlations (R'_{sp}) between the anomalies (seasonal cycle removed) of the
775 ESA CCI SM product (red) or CLM4.5 model (blue) and those of in situ observations
776 between 1993 and 2012 in the eight studied sub-regions of China using two evaluation
777 strategies (S1 and S2).

778 **Fig. 9** Averaged ubRMSD and R_{sp} values of the ESA CCI SM product against in situ
779 observations for five blended time periods. Red bars represent the sites with significant R_{sp}
780 values ($p < 0.05$) for all periods (1993–2012) while blue bars consider sites with significant
781 R_{sp} values ($p < 0.05$) for each blended period. Blend 3: July 1991–December 1997; Blend 4:
782 January 1998–June 2002; Blend 5: July 2002–December 2006; Blend 6: January
783 2007–September 2011; and Blend 7–8: October 2011–December 2012.

784 **Fig. 10** Evaluation of the ESA CCI SM product and CLM4.5 simulation against in situ
785 observations over different types of soil moisture stations. "All" is calculated using all valid
786 sites (200) with significant ($p < 0.05$) positive Spearman correlation coefficients for both the
787 ESA CCI SM product and CLM4.5 simulation. "Rain" represents the sites (101) located in
788 the same 0.25° grid box as the in situ precipitation observations; "No Rain" represents the
789 remaining sites (99). Presented are the average values, the standard deviations (as indicated
790 by the box), and the maximum and minimum values (whiskers).

791 **Fig. 11** Average statistical metrics: (a) ubRMSD, and (b) Spearman correlation coefficients
792 (R_{sp}) between the ESA CCI SM product (red) or in situ observations (OBS, blue) and
793 CLM4.5 simulation at different soil depths. "L1", "L1−2", "L1−2−3", "2cm", "5cm", and
794 "10cm" represent the first layer (0−1.75 cm), uppermost two layers (0−1.75, and 1.75−4.51
795 cm), and uppermost three layers (0−1.75, 1.75−4.51, and 4.51−9.06 cm), 0−2 cm, 0−5 cm,
796 and 0−10 cm, respectively. The average values of CLM4.5 were computed by using each soil
797 layer thickness as the weight; the CLM4.5 simulations were scaled to the dynamic range of

798 the in situ observations or ESA CCI SM dataset using a linear rescaling method (Eq. 1) prior
799 to computing the ubRMSD values.
800

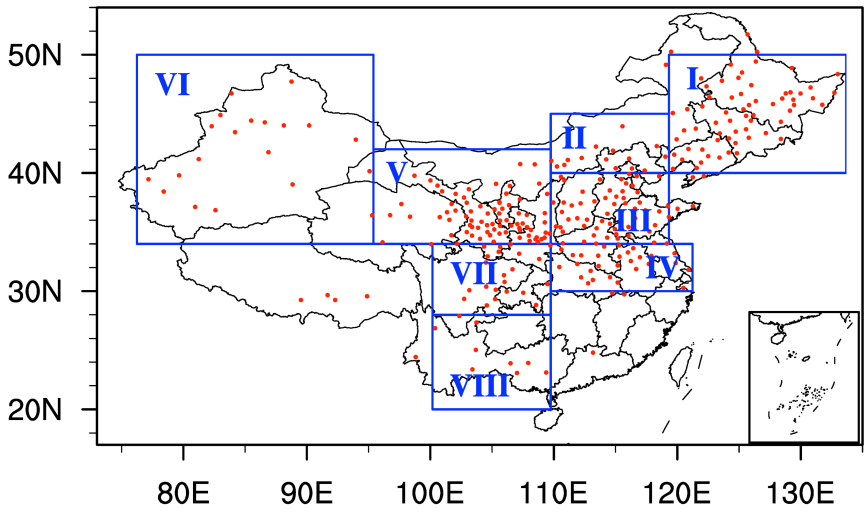

Fig. 1 Locations of the 306 in situ soil moisture measurement sites (red dots) in China. Also shown (blue boxes) are the eight sub-regions defined in Table 1.

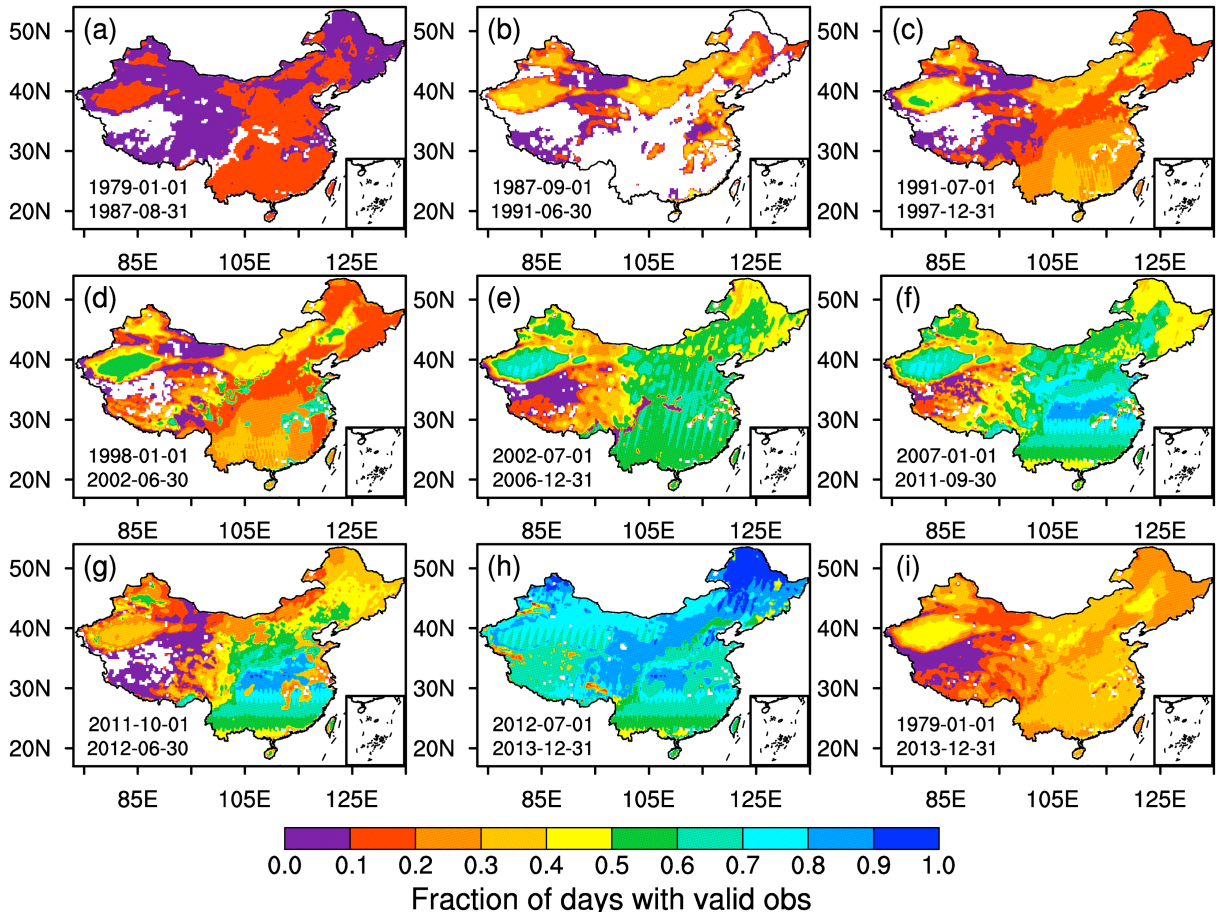

806

807 **Fig. 2** Fraction of days with valid observations, expressed as the number of days with
808 observations divided by the total number of days per period, split into six different merging
809 periods: (a) 1 January 1979–31 August 1987, (b) 1 September 1987–30 June 1991, (c) 1 July
810 1991–31 December 1997, (d) 1 January 1998–30 June 2002, (e) 1 July 2002–31 December
811 2006, (f) 1 January 2007–30 September 2011, (g) 1 October 2011–30 June 2012, (h) 1 July
812 2012–31 December 2013; and (i) for the total period 1 January 1979–31 December 2013.

813

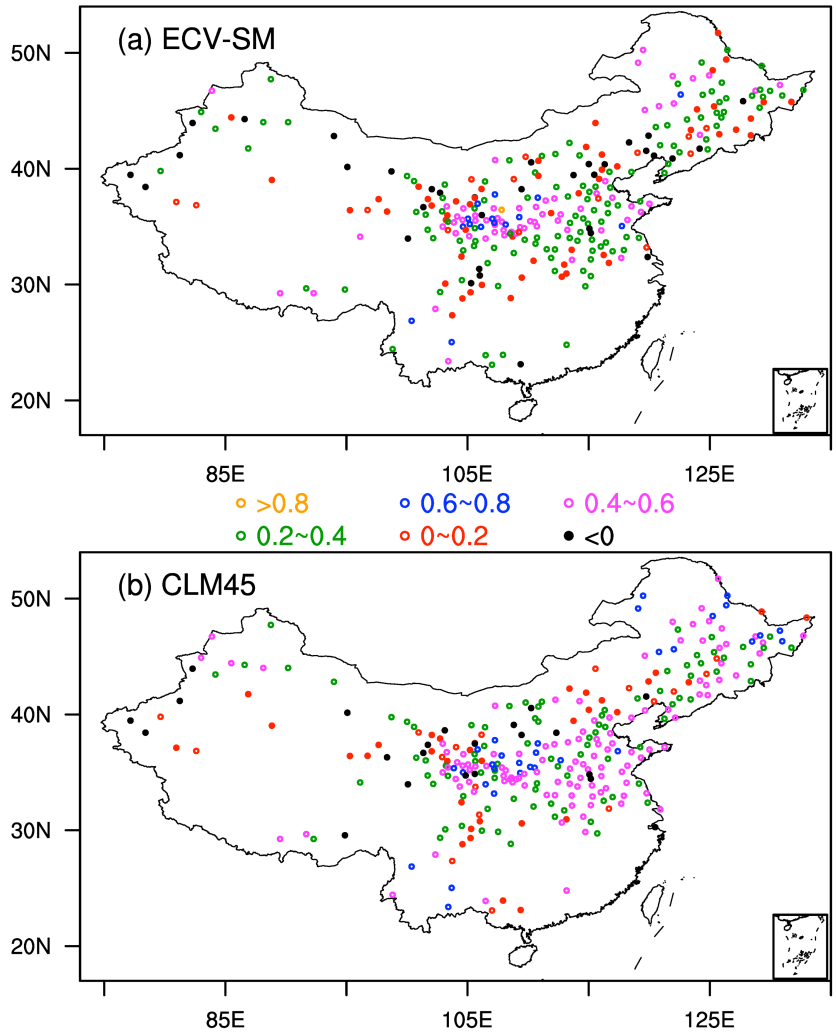

814

815 **Fig. 3** Spearman rank correlation coefficients (R_{sp}) between the in situ measurements and (a)
816 ESA CCI SM and (b) CLM4.5 from 1993 to 2012 at 306 sites in China. Open circles
817 represent statistically significant Spearman correlation ($p < 0.05$) while closed circles are not
818 significant.

819

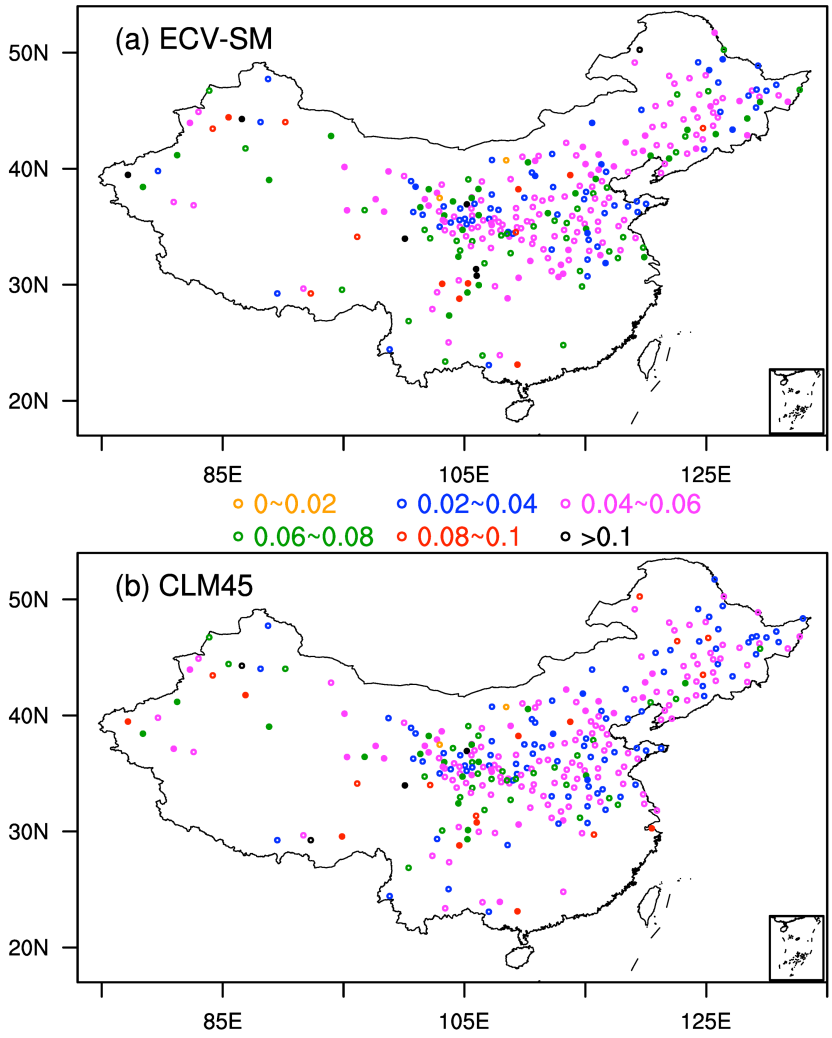

820

821 **Fig. 4** Unbiased root mean square differences (ubRMSDs) between the in situ measurements
822 and (a) ESA CCI SM and (b) CLM4.5 from 1993 to 2012 at 306 sites in China. Open circles
823 represent statistically significant Spearman correlation ($p < 0.05$) while closed circles are not
824 significant.

825

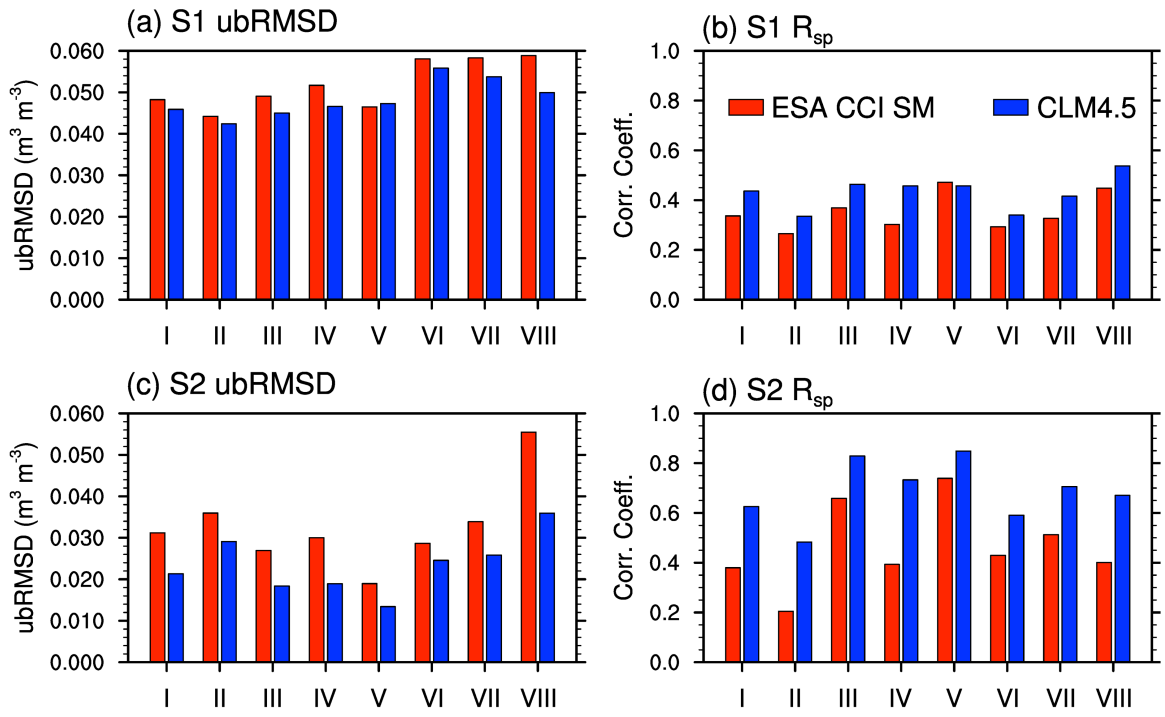

826

827 **Fig. 5** Statistical scores, including ubRMSD (5a and 5c) and R_{sp} (5b and 5d), for the ESA
828 CCI SM product (red) and CLM4.5 model (blue) between 1993 and 2012 in the eight studied
829 sub-regions of China using two evaluation strategies (S1 and S2). S1: average values of
830 statistical metrics for the stations over each region. S2: statistical metrics with in situ
831 observations for the soil moisture time series averaged at the stations of each region.

832

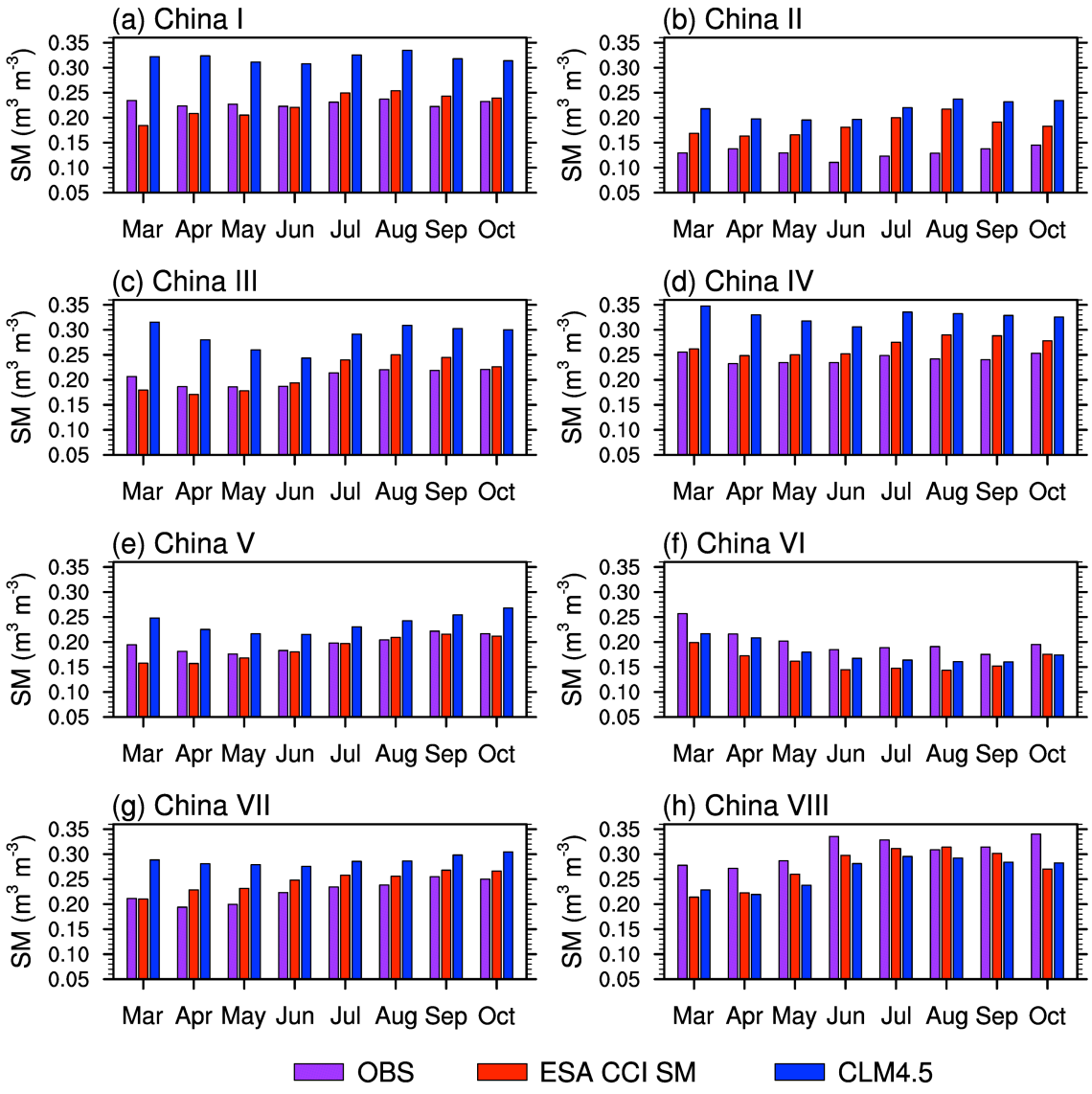

833

834 **Fig. 6** Multi-year (1993–2012) mean monthly volumetric soil moisture (SM, $m^3\ m^{-3}$) for the

835 period between March and October as described by in situ observations, the ESA CCI SM

836 product, and the CLM4.5 simulation in the eight studied sub-regions of China.

837

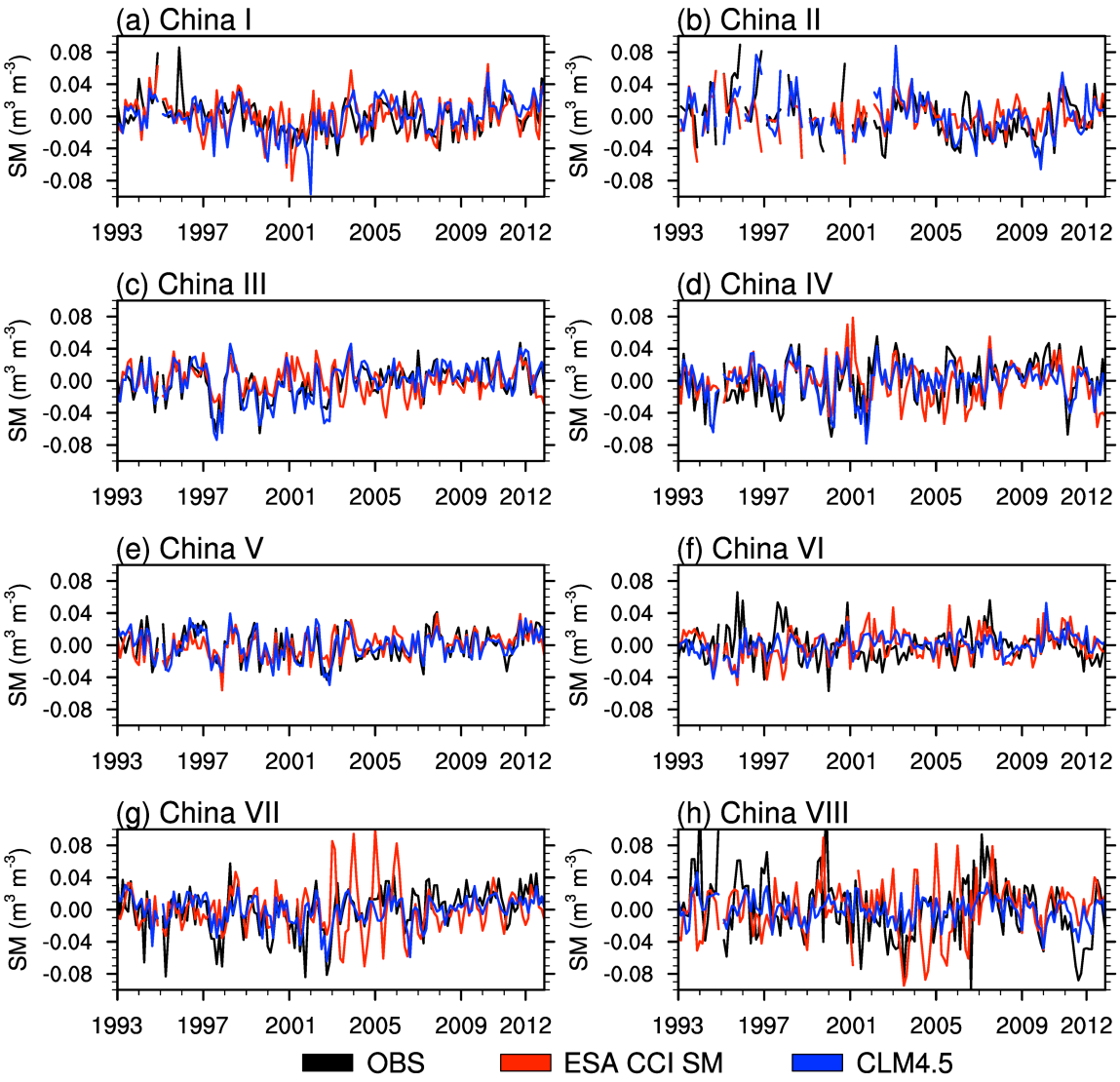

838

839 **Fig. 7** Comparison of the anomaly time series of monthly soil moisture derived from the ESA

840 CCI SM product, the CLM4.5 simulation, and in situ observations between 1993 and 2012

841 for the eight studied sub-regions of China.

842

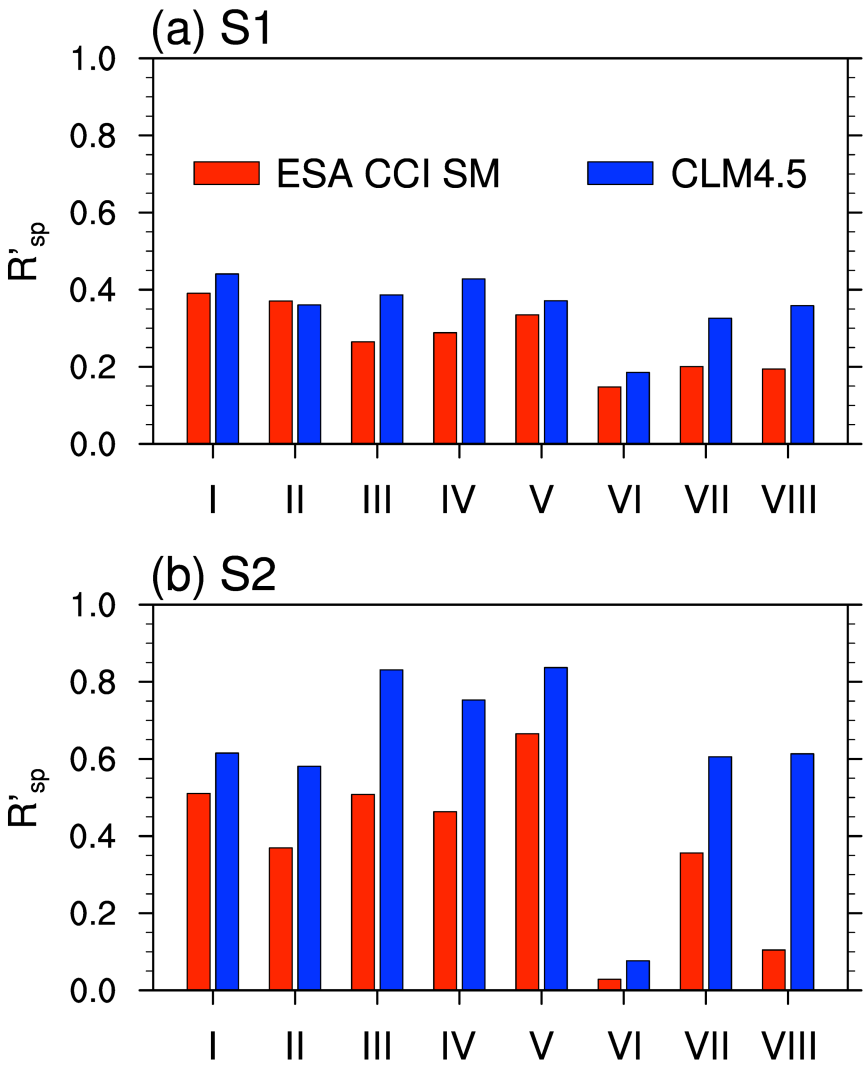

843

844 **Fig. 8** Spearman correlations (R'_{sp}) between the anomalies (seasonal cycle removed) of the
845 ESA CCI SM product (red) or CLM4.5 model (blue) and those of in situ observations
846 between 1993 and 2012 in the eight studied sub-regions of China using two evaluation
847 strategies (S1 and S2).

848

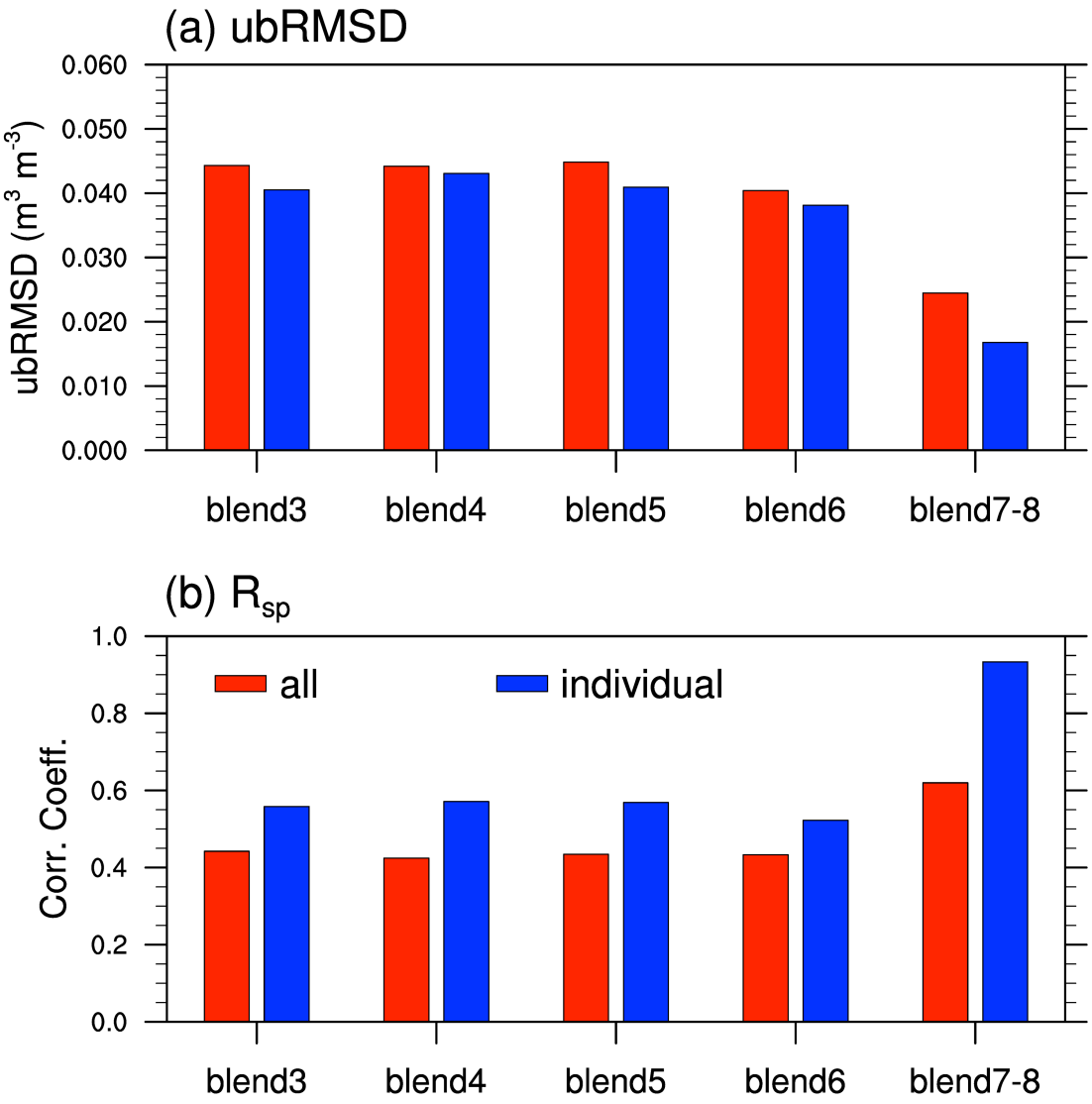

849

850 **Fig. 9** Averaged ubRMSD and R_{sp} values of the ESA CCI SM product against in situ
851 observations for five blended time periods. Red bars represent the sites with significant R_{sp}
852 values ($p < 0.05$) for all periods (1993–2012) while blue bars consider sites with significant
853 R_{sp} values ($p < 0.05$) for each blended period. Blend 3: July 1991–December 1997; Blend 4:
854 January 1998–June 2002; Blend 5: July 2002–December 2006; Blend 6: January
855 2007–September 2011; and Blend 7–8: October 2011–December 2012.

856

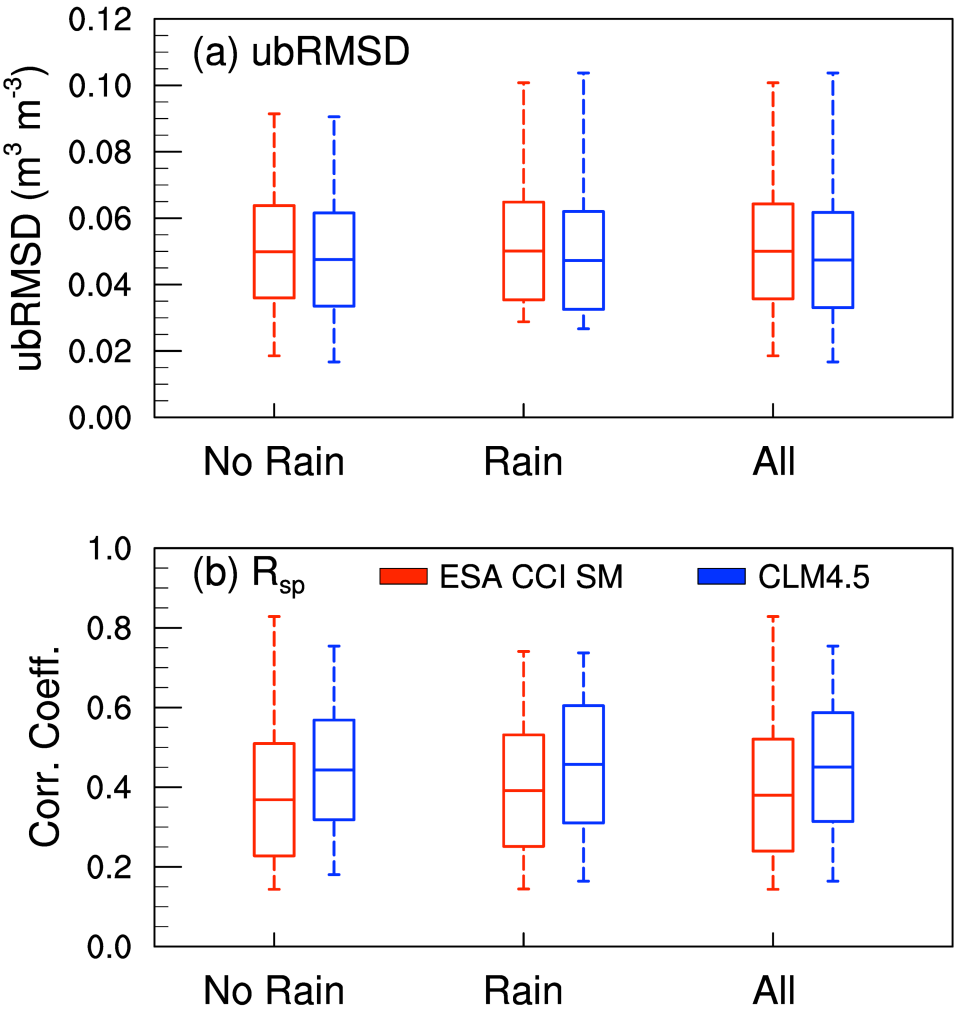

857

858 **Fig. 10** Evaluation of the ESA CCI SM product and CLM4.5 simulation against in situ
859 observations over different types of soil moisture stations. "All" is calculated using all valid
860 sites (200) with significant ($p < 0.05$) positive Spearman correlation coefficients for both the
861 ESA CCI SM product and CLM4.5 simulation. "Rain" represents the sites (101) located in
862 the same 0.25° grid box as the in situ precipitation observations; "No Rain" represents the
863 remaining sites (99). Presented are the average values, the standard deviations (as indicated
864 by the box), and the maximum and minimum values (whiskers).

865

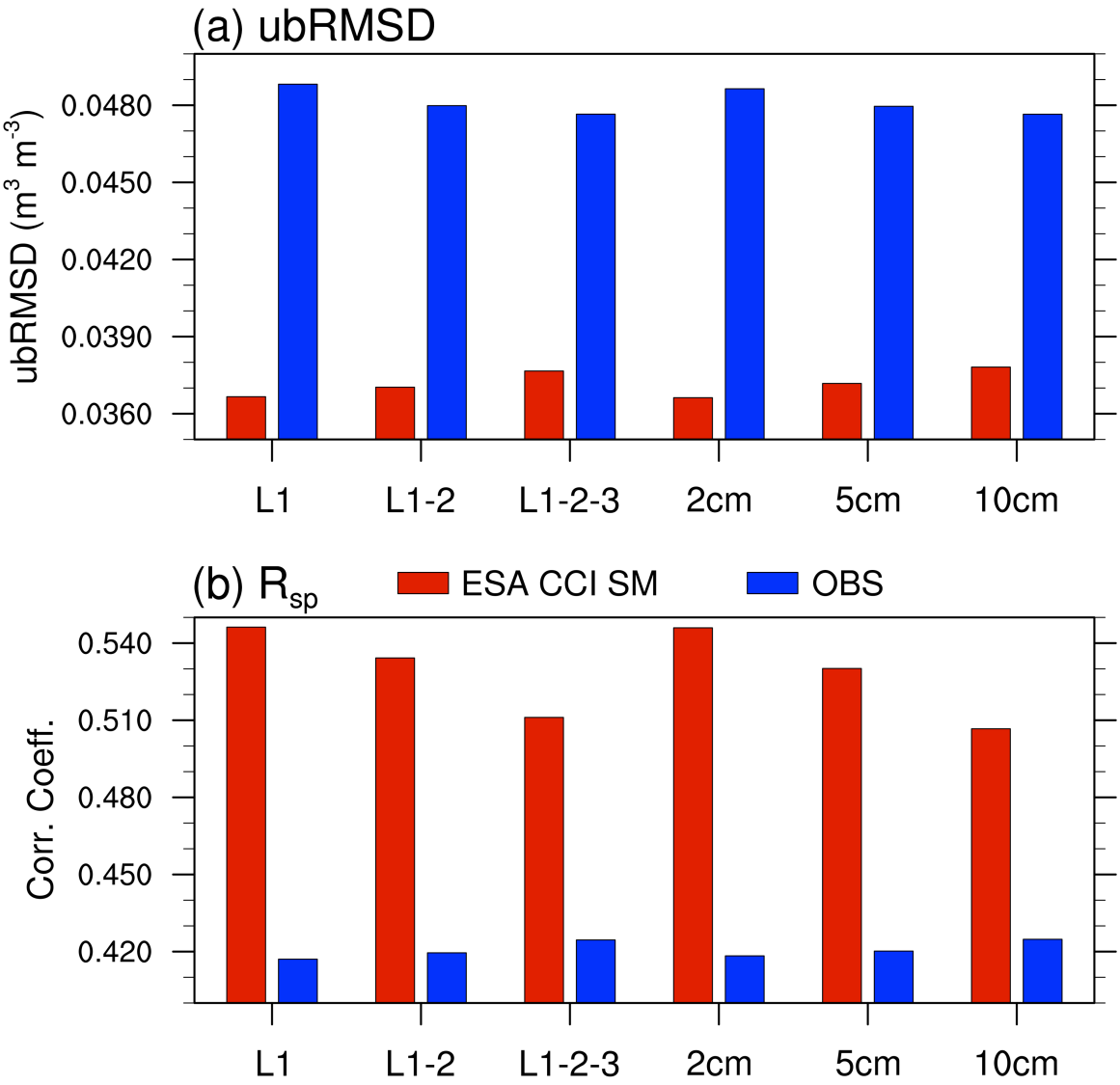

866

867 **Fig. 11** Average statistical metrics: (a) ubRMSD, and (b) Spearman correlation coefficients
868 (R_{sp}) between the ESA CCI SM product (red) or in situ observations (OBS, blue) and
869 CLM4.5 simulation at different soil depths. "L1", "L1−2", "L1−2−3", "2cm", "5cm", and
870 "10cm" represent the first layer (0−1.75 cm), uppermost two layers (0−1.75, and 1.75−4.51
871 cm), and uppermost three layers (0−1.75, 1.75−4.51, and 4.51−9.06 cm), 0−2 cm, 0−5 cm,
872 and 0−10 cm, respectively. The average values of CLM4.5 were computed by using each soil
873 layer thickness as the weight; the CLM4.5 simulations were scaled to the dynamic range of
874 the in situ observations or ESA CCI SM dataset using a linear rescaling method (Eq. 1) prior
875 to computing the ubRMSD values.